Marker-Assisted Image-Based 3D Monitoring for Active Catheters

A E T Yang, J. Szewczyk

Marker-Assisted Image-Based 3D Monitoring for Active Catheters

A.E.T. Yang[1], J. Szewczyk[1]

[1]*Institut des Systèmes Intelligents et de Robotique, Sorbonne Université*

yang@isir.upmc.fr

INTRODUCTION

Active catheters[1] for minimally invasive surgeries (MIS) have been increasingly studied for their dexterity, stability, and safety[2]. Accurate performance of MIS requires intra-operative feedback on catheter position and configuration in real-time. Many of the current catheter-monitoring technologies (image-based, motion-sensing, kinetic modeling, etc.) focus on tracking the position of the tip[3]. While information of the tip generally suffices for passive catheters, for active catheters, the additional degrees-of-freedom associated with deformation necessitate tracking of an extended longitudinal section. Otherwise, unmonitored active components along the length may operate unintendedly and cause tissue damages or punctures.

The full-length 3D configuration of an active catheter can be described by its shape and orientation. The present study aims to obtain both with fluoroscopy, which has been a standard protocol for catheter monitoring[4] for its wide adoption and relative simplicity. Nevertheless, fluoroscopic images are limited to 2D. In the absence of depth, the magnitude and direction of deflection may become undetectable, unless the deflection occurs perfectly parallel to the imaging plane. To overcome the limitations of 2D, previous image-based work achieved extended-length tracking of active catheters with bi-plane imaging[5], at the expense of additional imaging devices and computational effort.

Introducing radiopaque markers may reduce the cost. Publications have shown that band markers in fluoroscopy aid tip orientation tracking[6] and that helically-wrapped optical fibers aid curvature sensing[7]. This work attempts to train a shallow neural network (NN) to reconstruct full 3D configurations from marker projections in isolated images. The helical markers were adapted from existing components of a catheter that has been validated *in vivo*[8] (Fig. 1A). The system can potentially be generalized beyond fluoroscopy by substituting marker materials, such as echogenic markers for ultrasound[9][10] and radiofrequency coil for magnetic resonance imaging (MRI)[11].

MATERIALS AND METHODS

A prototype was made from a torque coil and compression springs (Fig. 1B) to mimic the active catheter in [8] at a scale of ~2x. An additional copper wire was looped around one end of the coil to serve as a reference for base point. Images of the prototype in various configurations (orientations and shapes) were acquired by Siemens' radiology system, Artis zeego.

The orientation of the catheter can be defined by yaw, roll, and pitch angles (Fig. 2A), and its shape can be approximated by a global bending angle taken between the most proximal and most distal sections (Fig. 2B). This preliminary study focused on two of the variables:

- θ_{roll}**:** varied automatically for a range of 56.4° in 142 increments as the imaging device rotated.
- θ_{bend}**:** varied manually among five angles (in Fig. 4), quantified when the imaging plane was parallel to the plane enclosing the bent catheter.

There were thus a total of 710 configurations. Note that in a realistic case, an operational active catheter has much higher number of possible θ_{bend}.

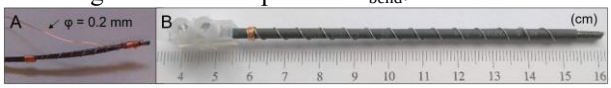

Fig. 1 (A) The active catheter (without cover) in [8]. **(B)** The prototype of catheter and markers implemented in this study.

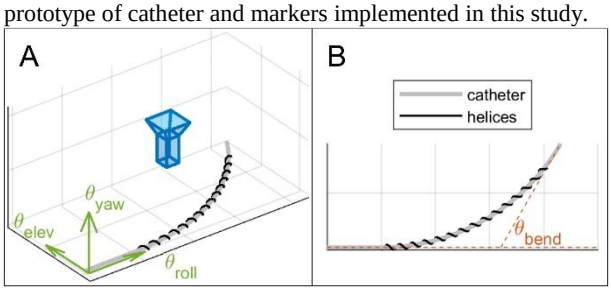

Fig. 2 (A) Three variables for orientation with respect to the imaging plane (in blue), and **(B)** one for shape.

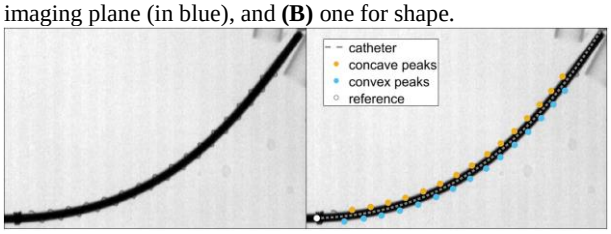

Fig. 3 An example of the original image (*left*) and the image overlaid with extracted features (*right*).

All images were processed in MATLAB™. Fig. 3 shows an example before and after feature extraction. The first step approximated the projected catheter as a 3rd-order polynomial. Next, the pixel furthest from the catheter within each region of connected pixels in proper sizes was identified as a "peak". Depending on projection perspective, not all peaks displayed as closed areas to be identifiable with the previous method. Hence, another method, based on the Qhull algorithm[12], looked for peaks from points forming the greatest convex hull encapsulating the catheter. Processing of each frame concluded with the elimination of falsely identified peaks and overlaps by thresholding inter-peak and peak-to-catheter distances. The trajectories of peaks are shown in Fig. 4 after interpolation between frames to compensate

for sporadically missing peaks. Each catheter configuration yielded 14 convex peaks and 14 concave.

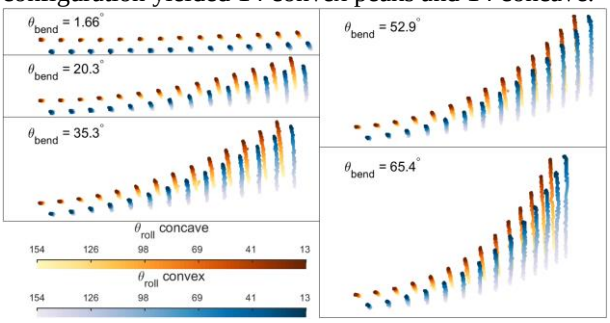

Fig. 4 The trajectories of projections of peaks at different θ_{roll} (*colors*) and θ_{bend} (*subplots*) (same x-axis limit for all).

RESULTS

To consolidate information, the 28 x- and y- values of peaks in each frame were converted into single predictors (variables of distances and slopes). For NN to uniquely recognize the two variables (θ_{bend} and θ_{roll}), a minimum requirement of two predictors are expected.

A two-layer feedforward NN was trained with a nonlinear least square fitting algorithm[13]. Data from all frames were divided randomly into training (70%), validating (15%), and testing (15%) sets. Among 10 tested predictors, the pair resulting in best results were:

- α_e (angle between tip and base slope)
- $\overline{d}_i$ (average inter-peak distances).

The correlations between NN-predicted and actual θ_{bend} and θ_{roll} of the testing set (n = 107) are depicted in Fig. 5A. Both angles have an average error of ~1° (Fig. 5B), and neither of the errors exhibited trend of variation.

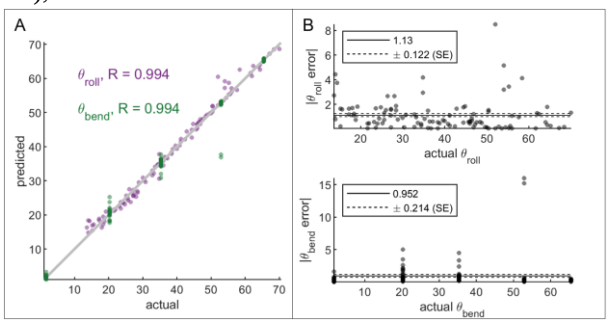

Fig. 5 (A) The correlations of θ_{roll} and θ_{bend} between NN prediction and ground truth. **(B)** The errors of θ_{roll} (*top*) and θ_{bend} (*bottom*), with means and standard errors in legends.

DISCUSSION

This paper demonstrated the potential of a system composed of designed radiopaque markers and neural network for efficient shape and orientation recognition of 3D catheters via single-plane fluoroscopy. A significant contribution of the system is its capability to detect high values of θ_{bend} even when θ_{bend} seems low in projections due to high θ_{roll} (e.g. bright markers in the last subplot in Fig. 4). Note that the results were achieved without regard to calibration of projection perspective.

Future work demands the inclusion of simulations on a comprehensive set of scenarios. Even though a simulation framework was initially utilized to guide the marker design and investigate the validity of the system, the NN in this paper was trained with experimental data, which limited the number of configurations. Coverage of a greater variety of θ_{bend} and θ_{roll} in NN training should robustize the performance of the NN. Moreover, the training data should also entail variations for θ_{pitch} and θ_{yaw}. Exploratory simulated results supported the efficacy of θ_{pitch} identification with the addition of one predictor. As for θ_{yaw}, parallel to the imaging plane, it is expected to be correlated with the overall x-y slopes. Experiments verifying θ_{pitch} and θ_{yaw} recognitions are ongoing.

Lastly, although for a certain types of active catheters, the helical markers may be easily or already incorporated as a component without altering the circumferential surface, it remains indispensable to examine the probable mechanical impact of markers during operation or insertion.

*This work was assisted by Dr. Pascal Haigron and Mr. Miguel Castro in image acquisition and supported by French state funds, ANR-11-LABX-0004.

REFERENCES

[1] Dario P et al. A miniature device for medical intracavitary intervention. In: Proceedings of IEEE Micro Electro Mechanical Systems. 1991. p. 171–5.

[2] Faddis MN et al. Magnetic guidance system for cardiac electrophysiology: a prospective trial of safety and efficacy in humans. J Am Coll Cardiol. 2003 Dec 3;42(11):1952–8.

[3] Rafii-Tari H et al. Current and Emerging Robot-Assisted Endovascular Catheterization Technologies: A Review. Ann Biomed Eng. 2014 Apr 1;42(4):697–715.

[4] Metz CE, Fencil LE. Determination of three-dimensional structure in biplane radiography without prior knowledge of the relationship between the two views: Theory. Med Phys. 1989;16(1):45–51.

[5] Baert SAM et al. Three-dimensional guide-wire reconstruction from biplane image sequences for integrated display in 3-D vasculature. IEEE Trans Med Imaging. 2003 Oct;22(10):1252–8.

[6] Hwang S, Lee D. 3D Pose Estimation of Catheter Band Markers based on Single-Plane Fluoroscopy. In: Proceedings of International Conference on Ubiquitous Robots. 2018. p. 723–8.

[7] Xu R et al. Curvature, Torsion, and Force Sensing in Continuum Robots Using Helically Wrapped FBG Sensors. IEEE Rob Autom Lett. 2016 Jul;1(2):1052–9.

[8] Couture T, Szewczyk J. Design and Experimental Validation of an Active Catheter for Endovascular Navigation. J Med Devices. 2017 Nov 22;12(1):011003-011003–12.

[9] Stoll J et al. Passive Markers for Tracking Surgical Instruments in Real-Time 3-D Ultrasound Imaging. IEEE Trans Med Imaging. 2012 Mar;31(3):563–75.

[10] Guo J et al. Ultrasound-Assisted Guidance With Force Cues for Intravascular Interventions. IEEE Trans Autom Sci Eng. 2019 Jan;16(1):253–60.

[11] Zuehlsdorff S et al. MR coil design for simultaneous tip tracking and curvature delineation of a catheter. Magn Reson Med. 2004 Jul 1;52(1):214–8.

[12] Barber CB et al. The Quickhull Algorithm for Convex Hulls. ACM Trans Math Softw. 1996 Dec;22(4):469–483.

[13] Hagan MT, Menhaj MB. Training feedforward networks with the Marquardt algorithm. IEEE Trans Neural Networks. 1994 Nov;5(6):989–93.